Plasma spraying of Fe-Cr-Al alloy powder

K. Voleník[1]*, O. Schneeweiss[2], J. Leitner[3], B. Kolman[1], J. Písačka[1]

[1]*Institute of Plasma Physics AS CR, v.v.i., Za Slovankou 3, 182 00 Prague 8, Czech Republic*
[2]*Institute of Physics of Materials AS CR, v.v.i., Žižkova 22, 616 62 Brno, Czech Republic*
[3]*Institute of Chemical Technology, Department of Solid State Engineering, Technická 5, 166 28 Prague 6, Czech Republic*

Received 14 June 2007, received in revised form 26 October 2007, accepted 26 October 2007

Abstract

Fe-Cr-Al alloy powder was plasma sprayed using a water stabilized plasma gun. The alloy simulated the commercial KANTHAL D. To obtain its composition in a plasma deposit, the initial powder composition must have been somewhat different to cope with the changes due to selective vaporization and selective oxidation during spraying. For the changes at the in-flight stage of spraying, mainly selective Al vaporization is responsible. After particle impact and solidification, i.e. during formation and cooling of a coating, vaporization is interrupted and the composition changes due to oxidation are less significant. During plasma spraying, the alloy exhibits better oxidation resistance than a number of materials. The protective mechanism is virtually the same as in solid Fe-Cr-Al alloys, nevertheless the protective Al_2O_3 layer is liquid under the reaction conditions.

K e y w o r d s: Fe-Cr-Al alloy powder, plasma spraying, oxidation, vaporization, composition changes

1. Introduction

Fe-Cr-Al alloys are frequently used in high temperature applications. They are usually fabricated as wires, strips or foils. It can be presumed that the alloy powders might be deposited by thermal spraying to form coatings on suitable substrates.

Bulk Fe-Cr-Al alloys and their properties have been studied extensively. Some recent papers are to be mentioned, describing various aspects of the alloy composition and behaviour and, in particular, the protective oxide layer growth. Among the Fe-Cr-Al-based alloys, some commercial KANTHAL materials and their behaviour have been reported [1, 2]. The resistance of Fe-Cr-Al alloys against high-temperature oxidation is ascribed to the formation of an alumina layer on the alloy surface, followed possibly by more complex multi-layered scales. In [3], a Fe-Al alloy has been chosen to show the influence of various Cr additions and the criteria for the formation of protective scales. The effects of minor additions and impurities in the alloys are reported in [4]. Other problems relating to the protective scales are dealt with in [5–8]. Some industrial applications of Fe-Cr-Al alloy are mentioned in [6]. In some cases, not only oxidation but also high temperature sulphidation resistance is of interest. In [9], the effect of Y addition to the alloy on the sulphidation behaviour has been studied.

In all the above given papers, bulk alloys and gas-solid high-temperature reactions have been investigated. Neither thermal spraying of powders nor the reactions gas-alloy melt have been mentioned.

Thermal spraying and, in particular, plasma spraying produces coatings composed of alloy splats. These are usually covered with thin oxide envelopes because atmospheric plasma spraying, which is the most widely used technique, is accompanied by oxidation due to air entrainment into the plasma gas. Larger oxide inclusions may appear too.

Two very different stages of the plasma spraying process must be taken into consideration. At the first (in-flight) stage, the molten powder particles move rapidly in the plasma flow. The second stage follows after hitting the substrate (particle solidification, coating formation and cooling down to room temperature).

*Corresponding author: tel.: +420 266 053 917; fax: +420 286 586 389; e-mail address: volenik@ipp.cas.cz

The first stage lasts some ≈ 10 ms, whereas the second one may take up more than 10 minutes.

During plasma spraying, the chemical composition of the alloy is usually changed. Two mechanisms contribute to this phenomenon:

– selective vaporization of elements during the flight of molten particles in the plasma flow, i.e. at the first (in-flight) stage of spraying,

– selective oxidation both at the first and at the second stages.

The relative contributions of the two mechanisms to the final alloy composition depend on a number of factors. For Fe-Cr and Ni-Cr alloys it has been stated that relatively more chromium was consumed by selective oxidation than by selective vaporization. In Fe-13%Cr and Ni-20%Cr, the loss of chromium with respect to iron or nickel due to selective vaporization did not exceed 0.3 %, whereas oxidation resulted in a decrease of ≈ 2.5 %. In Fe-15.6%Al, the situation was quite different. Some 5.5 % Al were lost by selective evaporation, while the effect of selective oxidation was much lower, about 1.3 % [10].

In the present paper, plasma spraying of a Fe-Cr-Al alloy is reported. The alloy composition was chosen so as to simulate approximately a KANTHAL-type material (in particular KANTHAL D) in order to reveal the peculiarities of its plasma spraying. The in-flight stage of spraying was of particular interest. In particular, it was desirable to reveal if the mechanism of high-temperature resistance of molten alloy drops is analogous to that of a solid alloy. With respect to the above mentioned composition changes, some deviations from the nominal concentrations of Cr and Al must have been presumed during spraying. It was highly probable that the Al content would fall considerably. That is why the Al concentration in the feedstock powder was increased by several % as shown below.

In contrast to the usual plasma spraying techniques, a water-stabilized plasma gun was employed [11, 12]. The scheme of the gun is shown in [13].

2. Experimental

2.1. Materials

The alloying elements in KANTHAL D are 22 % Cr and 4.8 % Al. To cope with the above mentioned decrease of Al concentration during plasma spraying, the Al content chosen in the feedstock powder was considerably higher. One of the problems was to have low levels of impurities in order not to be far from a ternary alloy. However, it is obvious that the impurities could not be fully eliminated. In the thermodynamic calculations (see below), no impurities could be taken into consideration. It was assumed that the impurities did not affect significantly the processes dealt with in this paper. To be able to compare the thermodynamic calculation results with the experiments, the impurities were neglected and the sum of Fe, Cr and Al concentrations was taken for 100 %. In this way, the results of chemical analysis were "renormalized", obtaining the values given below (section 4).

Table 1. Impurities (% by mass) in the Fe-Cr-Al feedstock powder

C	Co	Mn	N	Ni	O	Si
0.02	0.05	0.22	0.03	0.1	0.07	0.18

The actual impurity levels, obtained by the feedstock powder analysis, can be seen in Table 1.

To prepare the feedstock powder, the conventional "gas-atomizing" technique could not be applied. The preparation of the feedstock powder consisted in crushing pellets of the alloy. Ingots of the alloy were prepared by vacuum melting. To enable crushing by the available device, the ingots were melted again and the melt was poured into water to obtain pellets, though of irregular shape. After crushing, the size fraction $-0.14 +0.10$ mm was obtained by sieving. Several external laboratories took part in this complex powder preparation, in particular the ARA Company, Bratislava.

2.2. Plasma spraying

The powder particles were sprayed onto mild steel substrates by a 160 kW water-stabilized plasma gun WSP® Pal 160. The principle of the plasma gun function consists in heating and evaporation of water from the internal "wall" of the water vortex surrounding the d.c. arc. This is followed by water dissociation and ionization. The high-pressure plasma is blown from the nozzle to give rise to the plasma jet.

Characteristic distances: spraying distance SD (plasma gun nozzle – substrate) 400 mm, feeding distance FD (nozzle – powder injector) 65 mm. The powder throughput was $30\,\mathrm{kg\,h^{-1}}$.

Not only the composition of plasma deposits, but also that of the flying particles immediately before hitting the substrate were of interest. To conserve the composition of the particles after the in-flight period, it was necessary to cool down the flying particles (drops) abruptly at a point corresponding to the impact in current spraying runs and to stop any chemical reactions at the same point. For this purpose, the flying drops were trapped and quenched in liquid nitrogen. The average distance nozzle – liquid nitrogen level was ≈ 400 mm. However, the run started at a distance of 350 mm. The liquid nitrogen level fell rapidly during the spraying run lasting ≈ 15 s. The difference

between the nitrogen levels at the beginning and at the end of a spraying run was up to almost 100 mm. The feeding distance (nozzle – powder injector) was 65 mm. When removing the powder particles from liquid nitrogen, care must have been taken to avoid water condensation on the particle surface, which could result in surface corrosion.

As-sprayed plasma deposits were obtained after the second spraying stage. Mild steel plates were used as substrates.

2.3. Methods of analysis

Three types of samples were studied:

1. Feedstock powder before plasma spraying.
2. The product of the first spraying stage, i.e. the powder which passed through the plasma flow not hitting the substrate.
3. The plasma deposit after particle impact, solidification, coating formation and cooling down to the room temperature.

The feedstock powder, composed of metallic phases, was analysed by a conventional chemical method.

After the in-flight stage, the powder contained not only the alloy but also oxides grown during this stage. Each system containing metallic and oxide phases was analysed chemically as a whole to characterize the total concentration of the alloying element remaining in the particles after vaporization. To determine the alloy (not oxide) composition in the powder after the in-flight stage, cross sections of powder particles were investigated by X-ray microanalysis.

It was assumed that vaporization during the second spraying stage could be neglected. The cross sections of the deposit were prepared by a conventional metallographic technique. X-ray microanalysis of the metallic splats was then conducted.

All samples were studied by a scanning electron microscope CamScan 4DV and an energy dispersive X-ray microanalysis system LINK AN 10000. In each sample, cross sections of 10 alloy particles or splats were analysed to obtain the average concentration. The measured spots were as distant as possible from the particle surfaces, oxide layers or oxide inclusions. For details of the procedure including the calibration see [14].

For the qualitative phase analysis, X-ray diffraction (Co Kα radiation, $\lambda = 1.78901$ Å) as well as ^{57}Fe Mössbauer spectroscopy with detection of 14.4 keV gamma radiation in transmission mode were applied. The latter method also enabled revealing some details of the fine structure of the samples. As for the interpretation of diffraction data, the programme package HighScore Plus [15] was employed.

To estimate the amount of oxides in each sample, the oxygen level was measured by the LECO method ("extractive fusion"). However, the quantitative determination of the oxide amount from the results would not always be unambiguous. The nitrogen levels were measured by the same method.

The analysis of oxides was only possible after extracting them from the metallic samples. This was done by dissolving the metallic matrix using a technique described in [16]. After the first spraying stage, the as-sprayed powder was employed for this purpose. The plasma deposits after the second stage were treated by milling to obtain small chips suitable for metal dissolution.

3. Equilibrium calculations

Though the plasma processes are rapid, thermodynamic calculations have proven to give useful information on the composition of the reaction products [16]. During the in-flight stage at very high temperatures, the system is presumably not far from the thermodynamic equilibrium.

In particular, equilibrium calculations can predict the composition of metallic and oxidic phases in the system at the given conditions, especially the distribution of elements among all phases. However, as shown in [10], equilibrium calculations themselves are not able to explain the differing rates of evaporation of individual elements and, in the present case, the significant Al depletion at the first spraying stage. This is due to the fact that the evaporation rates depend not only on the equilibrium vapour pressure values, but mainly on the kinetic factors, in particular evaporation coefficients, which may change in a wide range in various species containing the same element.

A method based on minimizing the total Gibbs energy of the system for a set of points satisfying the material balance conditions was used to calculate the equilibrium composition of the systems Fe-Cr-Al-O-N-H for constant concentration values of Fe, Cr and Al in the alloy.

The equilibrium composition was calculated for various initial compositions of the gaseous phase. The plasma leaving the nozzle is composed of dissociated and ionized water vapour, however, due to air entrainment, the plasma is rapidly enriched in air. As the initial gaseous phase, water, air or a mixture of water-to-air 1 : 1 were taken into consideration, in all cases at atmospheric pressure (101.325 kPa). The calculations were conducted at constant temperatures in the range 1600–3200 K. The suggested initial amount of the solid phase was 10 moles. The initial relation of gas-to-solid molar amounts varied between 1 : 10 and 100 : 10. The former of these values corresponds to the case where all oxidizing species are consumed and some metallic phase remains in the system. On the other hand, the latter case means an almost unlimited delivery of oxygen, the system remains at approximately atmo-

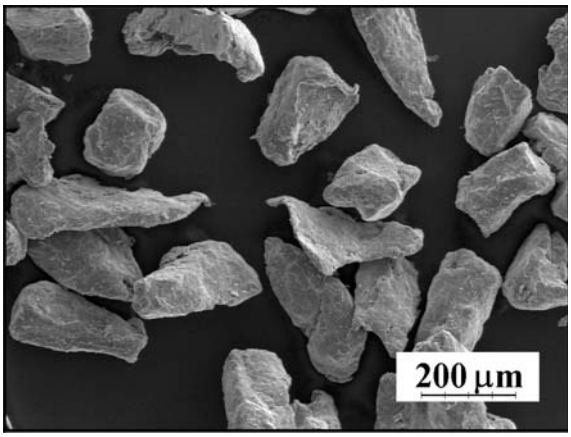

Fig. 1. Scanning electron micrograph of feedstock powder.

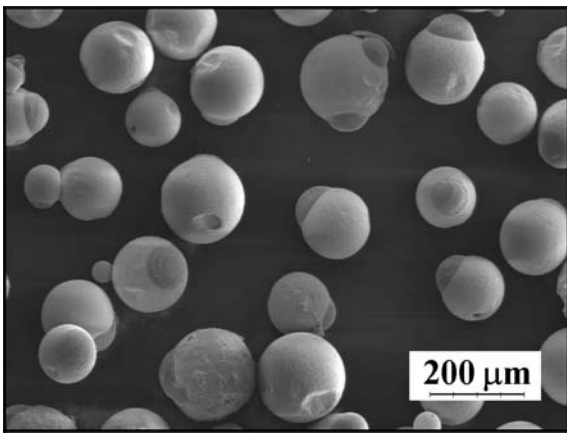

Fig. 2. Scanning electron micrograph of the particles after the 1st (in-flight) stage.

spheric pressure and all metallic phase is consumed. The real situation is suggested to correspond to some intermediate conditions, changing during the spraying run.

The solid oxides taken into consideration in the calculations were as follows:

Solid solutions of spinel-type oxides: $FeAl_2O_4$, $FeCr_2O_4$, Fe_3O_4,

Solid solutions of corundum-type oxides: Al_2O_3, Cr_2O_3, Fe_2O_3.

In addition, some other phases were taken into consideration, namely the gas phase, two liquid phases (metallic and oxidic), and fcc as well as bcc solid alloys.

4. Experimental results

4.1. Elemental composition of samples

Figures 1–3 show the scanning electron micrographs of feedstock powder, of the particles after the first spraying stage and a cross section of the coating after the second stage, respectively. In the X-ray microanalysis of the metallic phase as described in 2.3, cross sections of both powder types (not shown among the figures) and of the coating in the area imaged in Fig. 3 were investigated.

Table 2 gives the elemental composition, i.e. the concentration values of the alloying elements (% by mass) in the samples. Their sum together with the base element (Fe) is normalized to 100 %.

In Table 3, the results of oxygen determination (% by mass) are given. To show that the Fe-Cr-Al alloy is relatively resistant against oxidation during plasma spraying, published and even not yet published data obtained from some other alloys sprayed at approximately the same conditions are also given in Table 3.

The order of magnitude of the impurity levels was 0.1 % in all alloys (even in steel AISI 410).

In addition to oxygen, the concentrations of nitrogen in the Fe-Cr-Al alloy were measured, too. The results were 0.039 % (feedstock powder), 0.50 % (powder after the 1st spraying stage) and 0.38 % (coating). It can be seen that not only oxygen but also nitrogen content increased during plasma spraying, in particular at the first spraying stage. The molten particles

Table 2. Concentration values of the alloying elements in the Fe-Cr-Al alloy

Material	Sample	Concentration (% by mass)	
		Cr	Al
Feedstock powder	m. ph.	20.6	9.2
Powder after the first spraying stage	m. ph. with oxides	20.5	6.7
	m. ph.	19.8	5.2
Coating after the second stage	m. ph.	19.9	4.8

m. ph. = metallic phase

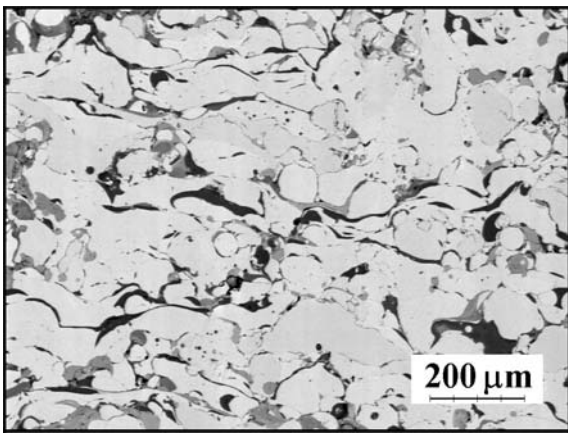

Fig. 3. Coating after the 2nd spraying stage (scanning electron micrograph of the cross section). The alloy is light grey, the oxides dark grey, pores and voids black.

Table 3. Oxygen levels in the Fe-Cr-Al alloy samples

Sample	Material	Oxygen concentration (% by mass)
Feedstock powder	A	0.069
	B	0.074
	C	0.06
	D	0.10
Powder after the 1st spraying stage	A	0.49
	B	0.67
	C	0.97
	D	1.8
Coating after the 2nd spraying stage	A	0.82
	B	1.7
	C	3.4
	D	4.5

A Fe-Cr-Al (this paper)
B Fe-15.5%Al
C steel AISI 410 (Fe-13.3%Cr)
D Ni-20.0%Cr [17]

seem to react with atmospheric nitrogen. An additional reaction takes place at the moment of hitting the liquid nitrogen level, which does not occur during conventional coating deposition by spraying.

4.2. Alloy structure

The phases composing both the alloy and the oxides were studied by X-ray diffraction and Mössbauer spectroscopy.

The alloy, according to qualitative X-ray diffraction analysis, was composed of the ferritic phase in all cases.

The interpretation of the Mössbauer spectra of the

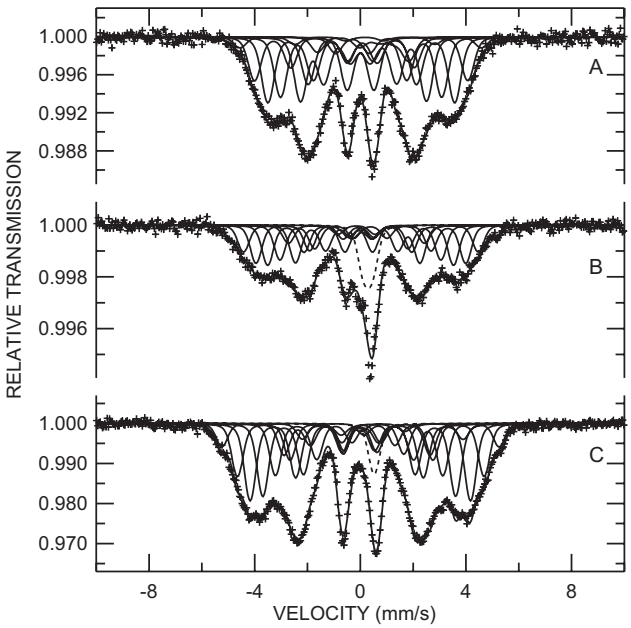

Fig. 4. Mössbauer spectra of Fe-Cr-Al alloy. A – feedstock powder, B – powder after the 1st spraying stage, C – coating after the 2nd spraying stage.

alloy (Fig. 4) was based on the values of the hyperfine induction B_{Hf} calculated from the magnetic splitting of all spectrum components, taking into account their intensities. The magnetic splitting of a component results in a sextet. Each sextet corresponds to one type of the nearest neighbourhood of any iron atom in the alloy lattice. Qualitatively, the higher the number of non-ferrous atoms in the neighbourhood (i.e. in the first coordination sphere), the lower the B_{Hf} value. Besides, there is another strong effect. If B_{Hf} is low, particularly 18.6 T in the feedstock powder (Fig. 4A), it suggests the presence of an ordered Fe-Cr-Al alloy. The low value of B_{Hf} may result from a combination of alloying by Cr and Al and formation of $D0_3$(B2) superstructure.

During plasma spraying, the hyperfine induction gradually increased. In the powder after the in-flight stage, $B_{\mathrm{Hf}} = 21.8$ T (Fig. 4B), in the coating $B_{\mathrm{Hf}} = 24.2$ T (Fig. 4C). The increasing values of B_{Hf} in this sequence are due to the decreasing Al concentration (the changes of Cr content are small) and a lack of ordering. The single line component (dashed line) in the spectrum of the powder after the 1st and 2nd spraying stages (Figs. 4B,C) has the isomer shift $\delta = 0.38\,\mathrm{mm\,s^{-1}}$ (relative to α-Fe). It can be hardly attributed to any metallic phase present in the samples. The single line appears if a conventional fit of the spectra is applied. Another approach would perhaps suppress the single line, however, there does not seem to be a physical reason for any constraint.

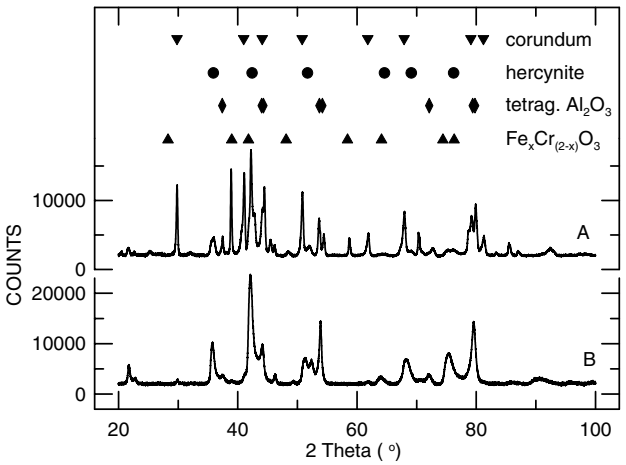

Fig. 5. X-ray diffraction pattern of oxides extracted from alloy powder. A – after the 1st spraying stage, B – after the 2nd spraying stage.

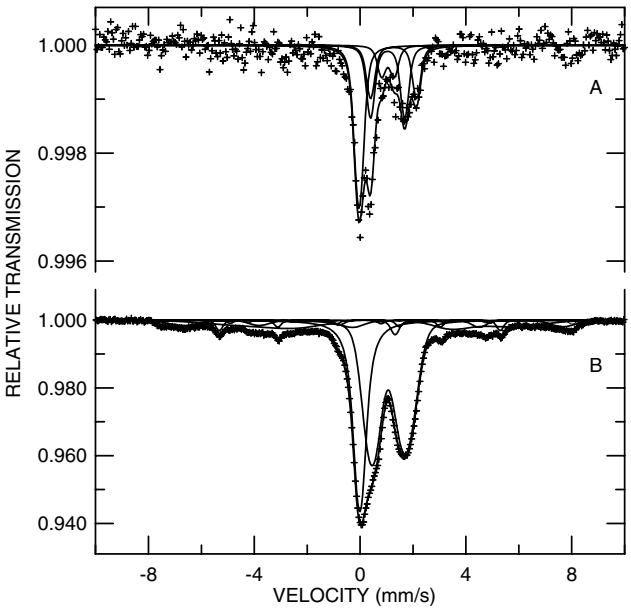

Fig. 6. Mössbauer spectra of oxides extracted from the Fe-Cr-Al alloy. A – after the 1st spraying stage, B – after the 2nd spraying stage.

4.3. Structure of oxides

In the oxidation products separated from the alloy after the 1st and 2nd spraying stages, four oxide types were identified by X-ray diffraction: corundum, hercynite $FeAl_2O_4$, tetragonal Al_2O_3 (ICSD Ref. Code 01-080-0956 [18]), and $Fe_xCr_{(2-x)}O_3$ where $x \approx 1.2$ (rhombohedral, ICSD Ref. Code 00-034-0412) as shown in Fig. 5. The Mössbauer spectra (Fig. 6) indicate that the iron-containing oxides were composed mainly of hercynite. Its component is formed by a broad asymmetric doublet. This component was obtained by its fitting using quadrupole splitting distribution which can be explained by deviations from the stoichiometric composition. Beside the hercynite spectrum component, an additional line – singlet – is detected in the spectra. Its isomer shift $\delta = -0.05 \pm 0.01$ mm s^{-1} is in good agreement with the component identified in [19] and can be attributed to iron clusters embedded in a paramagnetic oxide matrix. Pure Al_2O_3 and Cr_2O_3 are not detectable by Mössbauer spectroscopy.

Some amounts of Fe^{3+} and Fe^{2+} present in non-specified oxide phases were also found. The phases may be $(Fe^{3+}Cr^{3+}Al^{3+})_2O_3^{2-}$ containing trivalent Fe, and $Fe^{2+}(Fe^{3+}Cr^{3+}Al^{3+})_2O_4^{2-}$ where also divalent iron ions are located. The spectrum in Fig. 6B also shows hardly detectable magnetically split components showing the presence of undissolved alloy remainders and a very small amount of an oxide suggesting Fe_3O_4.

As mentioned above, all the oxide samples were separated (extracted) from the alloy phase prior to structure investigation. As a rule, a mixture of oxide phases was obtained. To study the individual oxides and their composition and structure, a technique enabling separation of oxide phases from each other must have been available, which was not the case. It is obvious that X-ray diffraction measurement of lattice parameters would be of little value in this complex system.

5. Results of equilibrium calculations

Summarizing the results of thermodynamic calculations, it can be stated that not only the alloy but also all the oxides taken into consideration are liquid at $\geq$ 2400 K. To identify the solid phases appearing during rapid cooling of the particles, lower temperatures are relevant.

Though the principle spraying conditions (plasma composition, particle composition, particle temperature) change during the in-flight period, they must be considered strictly constant in equilibrium calculations. Thus, it was necessary to choose a wide range including all possible conditions and to consider qualitatively the results obtained for a set of intermediate cases. An example, in which all species are molten, is in Table 4.

If the sum of element percentages in both melt types is less than 100 %, the remaining amount is in the vapour phase. These values are significant at higher temperatures than 2400 K.

At 1600 K, all other conditions being the same as in Table 4, the oxides are solid. This is the lowest temperature involved in the calculations. The sample

Table 4. Equilibrium calculation results (% of each element in both melt types in relation to the initial concentrations in the alloy) for the water-to-air mixture 1:1 at the in-flight stage at 2400 K. The initial number of moles of the solid phase was 10 in all cases

Melt type	Element	Initial proportion of phases (gas (mole):sol (mole))		
		0.1	1	10
Metallic	Al	71.81	0.02	< 0.01
	Cr	99.63	19.59	< 0.01
	Fe	99.86	74.47	< 0.01
Oxidic	Al	27.48	99.98	100.00
	Cr	< 0.01	78.84	96.81
	Fe	< 0.01	23.58	99.66

Table 5. Equilibrium calculation results (number of moles of each oxide) for the water-to-air mixture 1:1 at the in-flight stage at 1600 K and gas (mole):sol (mole) = 1. The initial number of moles of the solid phase was 10 in all cases

Oxide		Content (mole)
Corundum-type	Al_2O_3	0.37
	Cr_2O_3	0.10
	Fe_2O_3	< 0.01
Spinel-type	$FeAl_2O_4$	0.48
	$FeCr_2O_4$	0.88
	Fe_3O_4	< 0.01

temperature falls rapidly to this value during cooling, be it after the 1st or after the 2nd plasma spraying stage. In the former case, very rapid cooling continues and all reactions are interrupted. In the latter case, some changes may still occur during building up the coating, mainly due to further oxidation. In Table 5, the values calculated for all oxides taken into consideration are given.

Another extreme case is 3200 K. If all other conditions are the same as in Tables 4 and 5, the elements Al, Cr and Fe are distributed between the vapour phase and the oxidic melt. No metallic melt is present. However, the probable maximum surface temperature of the particles is considerably lower than 3200 K. There is a lack of experimental data of the surface temperature of metallic particles in a plasma stream produced by a water stabilized gun. Though ceramic particles certainly behave in a different way, it may be worth noting that the mean surface temperature of alumina 50–63 μm in size varied between 2570 and 2720 K at 250 mm from the nozzle for various particle trajectories. If increasing this distance by 150 mm, the resulting mean temperature drop was 130 K [20]. For a metallic powder (cast iron), the average temperature values were several hundreds of K lower.

The mean real value of gas: sol may be assumed approximately between 0.1 and 1.

6. Discussion

From the analyses of particles quenched in liquid nitrogen as well as of plasma deposits it follows that the alloy Fe-Cr-Al is highly resistant against oxidation during plasma spraying as compared with other Fe- or Ni-based alloys. This concerns both the melt at the in-flight stage and the solid alloy after impact. The corrosion and oxidation resistance of thermally sprayed coatings can of course never reach the levels typical of bulk alloys because of the presence of defects, in particular pores and oxide inclusions, in the coatings.

With respect to the losses of reactive elements during plasma spraying due to selective evaporation and oxidation, it is a difficult task to choose their initial concentrations. In the present paper where one of the aims was to obtain alloy coatings from an alloy simulating KANTHAL D, the choice of Al concentration was successful. However, the Cr concentration was somewhat lower than in KANTHAL D.

For the alloy under consideration, the equilibrium vapour pressure of Al is, in general, lower than that of Cr or Fe. It appears that the kinetics of Al selective vaporization depends more significantly on the evaporation coefficient, which is unknown for the given alloy, than on the equilibrium vapour pressure.

In the feedstock powder as well as the samples after both stages of plasma spraying, the alloy structure was bcc (α-phase). The σ-phase, which may appear in Fe-Cr alloys at low temperatures, was not found. This is in agreement with a diagram published as early as in 1964 in [21] where it can be seen that the compositions under consideration are outside the region in which the σ-phase (or $\alpha + \sigma$) may exist. The low hyperfine induction, in particular in the feedstock powder, suggests some kind of ordering similar to Fe_3Al. A partially ordered structure also resulted from the in-flight stage.

The solid oxide structures may be taken for a superposition of species appearing during plasma spraying of Fe-Cr and Fe-Al alloys. Among the oxide phases detectable by Mössbauer spectroscopy, hercynite $FeAl_2O_4$ was dominant. The presence of complex oxides, corundum-type $(Fe,Cr,Al)_2O_3$ and spinel-type $(Fe,Cr,Al)_3O_4$ is possible, however, they cannot be determined unambiguously by the existing methods.

Similarly as in Fe-Al alloys, preferential oxidation of Al at the in-flight stage results in a thin film of molten Al_2O_3. This film is responsible for a good oxidation resistance of molten particles. However, at a late period of the in-flight stage, the Al-oxide melt is mostly blown to the rear part of the flying molten alloy drop resulting in an almost hemisperical "cap" on the particle surface after solidification [22] and leaving a free area on the remaining drop surface. Several "caps" of this type can be seen in Fig. 2. They were analysed by X-ray microanalysis by which virtually only Al was found, whereas the concentrations of Fe and Cr were < 1 % in all cases. It follows that the "caps" were composed of almost pure Al_2O_3. The free surface allowed enhanced evaporation and possible formation of more complex oxides.

7. Conclusions

1. Plasma spraying of an alloy Fe-Cr-Al was studied. The alloy composition was chosen so as to simulate approximately KANTHAL D. However, with respect to the rapid selective vaporization of Al observed previously, the concentration of this element chosen for the feedstock powder was considerably higher than in KANTHAL D.

2. During the two stages of plasma spraying, the Al concentration fell to the value corresponding to KANTHAL D.

3. The oxidation resistance of the Fe-Cr-Al alloy is high as compared with a number of binary alloys. It was shown that the reason for the good resistance is virtually the same as in solid Fe-Cr-Al alloys referred to in the literature, nevertheless the protective Al_2O_3 layer is liquid under the reaction conditions.

4. Semi-spherical "caps" of solidified Al-oxide are frequently observed on the surface of solidified drops, which is due to drag forces transferring most of the oxide melt to small areas at the rear parts of the flying drops. This occurs at the late period of alloy particle flight.

Acknowledgements

This work was supported by the Academy of Sciences of the Czech Republic, Institutional Research Project No. AV0Z20430508 and grant IAA1041404.

References

[1] JOSEFSSON, H.—LIU, F.—SVENSSON, J. E.—HALVARSSON, M.—JOHANSSON, L. G.: Materials and Corrosion – Werkstoffe u. Korrosion, *56*, 2005, p. 801.

[2] BENNETT, M. J.—NICHOLLS, J. R.—SIMMS, M. J.—NAUMENKO, D.—QUADAKKERS, W. J.—KOCHUBEY, V.—FORDHAM, R.—BACHORCZYK, R.—GOOSSENS, D.—HATTENDORF, H.—SMITH, A. B.—BRITTON, D.: Materials and Corrosion – Werkstoffe u. Korrosion, *56*, 2005, p. 854.

[3] ZHANG, Z. G.—GESMUNDO, F.—HOU, P. Y.—NIU, Y.: Corrosion Sci., *48*, 2006, p. 741.

[4] KOCHUBEY, V.—AL-BADAIRY, H.—TATLOCK, G.—LE-COZE, J.—NAUMENKO, D.—QUADAKKERS, W. J.: Materials and Corrosion – Werkstoffe u. Korrosion, *56*, 2005, p. 848.

[5] HOU, P. Y.—ZHANG, X. F.—CANNON, R. M.: Scripta materialia, *50*, 2004, p. 45.

[6] QUADAKKERS, W. J.—NAUMENKO, D.—WESSEL, E.—KOCHUBEY, V.—SINGHEISER, L.: Oxidation of Metals, *61*, 2004, p. 17.

[7] NYCHKA, J. A.—CLARKE, D. R.: Oxidation of Metals, *63*, 2005, p. 325.

[8] BERTHOME, G.—N'DAH, E.—WOUTERS, Y.—GALERIE, A.: Materials and Corrosion – Werkstoffe u. Korrosion, *56*, 2005, p. 389.

[9] PILLIS, M. F.—RAMANATHAN, L. V.: Corrosion Prevention & Control, *50*, 2003, p. 167.

[10] LEITNER, J.—VOLENÍK, K.—NEUFUSS, K.—KOLMAN, B.: Czech. J. Phys., *56*, 2006, p. B1391.

[11] CHRÁSKA, P.—HRABOVSKÝ, M.: In: Proc. Int. Thermal Spray Conf. & Exposition 1992. Ed.: Berndt, C. C. Materials Park, OH, ASM Int. 1992, p. 81.

[12] HRABOVSKÝ, M.: Pure & Appl. Chem., *70*, 1998, p. 1157.

[13] VOLENÍK, K.—NOP, P.—KOPŘIVA, P.—KOLMAN, B.—DUBSKÝ, J.: Kovove Mater., *44*, 2006, p. 41.

[14] CHRÁSKA, P.—KOLMAN, B.—SUCHÁNEK, M.—VOLENÍK, K.: In: Proc. Int. Thermal Spray Conf. 2004. Eds.: Kuroda et al. Düsseldorf, Verlag für Schweißen und verwandte Verfahren, DVS-Verlag GmbH 2004 (CD-ROM).

[15] X'Pert HighScore Plus 2.0a, PANanalytical B. V., Almelo, the Netherlands.

[16] VOLENÍK, K.—LEITNER, J.—HANOUSEK, F.—DUBSKÝ, J.—KOLMAN, B.: J. Thermal Spray Technol., *6*, 1997, p. 327.

[17] VOLENÍK, K.—CHRÁSKA, P.—DUBSKÝ, J.—HAD, J.—LEITNER, J.—SCHNEEWEISS, O.: In: Proc. Int. Thermal Spray Conf. 2003. Eds.: Marple, B. R., Moreau, C. Materials Park, OH, ASM Int. 2003, p. 1033.

[18] ICSD Database, release 2004/1, FIZ Karlsruhe, Germany.

[19] PAESANO, A., Jr.—MATSUDA, C. K.—CÓTICA, L. F.—de MEDEIROS, S. N.—da CUNHA, J. B. M.—HALLOUCHE, B.—SILVA, S. L.: J. Applied Phys., *96*, 2004, p. 2540.

[20] CHRÁSKA, T.—NEUFUSS, K.—OBERSTE-BERGHAUS, J.—LAMONTAGNE, M.—MOREAU, C.: In: Proc. Int. Thermal Spray Conf. 2005. Eds.: Lug-

scheider et al. Düsseldorf, Verlag für Schweißen und verwandte Verfahren, DVS-Verlag GmbH, p. 1292 (CD-ROM).
[21] VULF, B. K.: Trojnye metallicheskie fazy v splavach. Moscow, Izd. Metallurgia 1964.
[22] VOLENÍK, K.—KOLMAN, B.—DUBSKÝ, J.—CHRÁSKA, P.: In: Proc. Int. Thermal Spray Conf. 2005. Eds.: Lugscheider et al. Düsseldorf, Verlag für Schweißen und verwandte Verfahren, DVS-Verlag GmbH, p. 1175 (CD-ROM).